

# Phenotypic Effects of Biglycan Deficiency Are Linked to Collagen Fibril Abnormalities, Are Synergized by Decorin Deficiency, and Mimic Ehlers-Danlos–Like Changes in Bone and Other Connective Tissues

A. CORSI,<sup>1</sup> T. XU,<sup>2</sup> X-D. CHEN,<sup>2</sup> A. BOYDE,<sup>3</sup> J. LIANG,<sup>2</sup> M. MANKANI,<sup>2</sup> B. SOMMER,<sup>2</sup> R.V. IOZZO,<sup>4</sup>  
I. EICHSTETTER,<sup>4</sup> P. GEHRON ROBEY,<sup>2</sup> P. BIANCO,<sup>5</sup> and M.F. YOUNG<sup>2</sup>

## ABSTRACT

Decorin (*dcn*) and biglycan (*bgn*), two members of the family of small leucine-rich proteoglycans (SLRPs), are the predominant proteoglycans expressed in skin and bone, respectively. Targeted disruption of the *dcn* gene results in skin laxity and fragility, whereas disruption of the *bgn* gene results in reduced skeletal growth and bone mass leading to generalized osteopenia, particularly in older animals. Here, we report that *bgn* deficiency leads to structural abnormality in collagen fibrils in bone, dermis, and tendon, and to a “subclinical” cutaneous phenotype with thinning of the dermis but without overt skin fragility. A comparative ultrastructural study of different tissues from *bgn*- and *dcn*-deficient mice revealed that *bgn* and *dcn* deficiency have similar effects on collagen fibril structure in the dermis but not in bone. Ultrastructural and phenotypic analysis of newly generated *bgn/dcn* double-knockout (KO) mice revealed that the effects of *dcn* and *bgn* deficiency are additive in the dermis and synergistic in bone. Severe skin fragility and marked osteopenia characterize the phenotype of double-KO animals in which progeroid changes are observed also in the skin. Ultrastructural analysis of bone collagen fibrils in bone of double-KO mice reveals a complete loss of the basic fibril geometry with the emergence of marked “serrated fibril” morphology. The phenotype of the double-KO animal mimics directly the rare progeroid variant of human Ehlers-Danlos syndrome (EDS), in which skin fragility, progeroid changes in the skin (reduced hypodermis), and osteopenia concur as a result of impaired glycosaminoglycan (GAG) linking to *bgn* and *dcn* core proteins. Our data show that changes in collagen fibril morphology reminiscent of those occurring in the varied spectrum of human EDS are induced by both *bgn* deficiency and *dcn* deficiency in mice. The effects of an individual SLRP deficiency are tissue specific, and the expression of a gross phenotype depends on multiple variables including level of expression of individual SLRPs in different tissues and synergisms between different SLRPs (and likely other macromolecules) in determining matrix structure and functional properties. (J Bone Miner Res 2002;17:1180–1189)

**Key words:** decorin, biglycan, collagen fibrils, double-knockout, Ehlers-Danlos

## INTRODUCTION

DECORIN (*dcn*) and biglycan (*bgn*) belong to the family of secreted small leucine-rich proteoglycans (SLRPs).<sup>(1–4)</sup> This family includes at least 12 different molecules that can

be divided into three distinct subfamilies based on similarities in amino acid sequences and gene organization. Their core proteins are composed of tandemly linked repeats of an ~25 amino acid leucine-rich sequence to which different glycosaminoglycan (GAG) chains are attached. However, alternative post-translational modifications of certain SLRP members also may result in the biosynthesis of mature

The authors have no conflict of interest.

<sup>1</sup>Department of Experimental Medicine, Università dell’Aquila, L’Aquila, Italy.

<sup>2</sup>Craniofacial and Skeletal Diseases Branch, National Institute of Craniofacial and Skeletal Diseases, National Institutes of Health, Bethesda, Maryland, USA.

<sup>3</sup>Department of Anatomy and Developmental Biology, University College London, London, United Kingdom.

<sup>4</sup>Department of Pathology, Anatomy and Cell Biology, Jefferson Medical College, Thomas Jefferson University, Philadelphia, Pennsylvania, USA.

<sup>5</sup>Department of Experimental Medicine and Pathology, La Sapienza University, Rome, Italy.

proteins more properly referred to as glycoproteins rather than proteoglycans.<sup>(3)</sup> To date, no primary genetic defects in either *DCN* or *BGN* have been reported in humans. However, steady-state levels of biglycan mRNA and protein are altered in cells derived from patients with anomalies of the X chromosome, where the biglycan gene is located.<sup>(5)</sup>

In most tissues, SLRPs are thought to regulate extracellular matrix structure and organization. They are postulated also to regulate cell growth and differentiation, mainly by modulating local storage and/or availability of different growth factors including transforming growth factor (TGF)  $\beta$ <sup>(4,6,7)</sup> and by interacting with receptor tyrosine kinases.<sup>(8)</sup> Various members of the SLRP family are known to interact directly with fibrillar collagen, thereby modulating fibril formation, growth, and morphology<sup>(9–16)</sup> in vitro.

However, detailed functions of each SLRP in vivo remain to be clarified. Differences in their interaction with collagens, GAG content, and, in particular, the different patterns of expression in different tissues may imply diverse, tissue-specific roles for each SLRP.<sup>(4,17)</sup> Some degree of tissue specificity indeed has been highlighted by the development of mouse models carrying targeted null mutations of individual SLRP genes. A phenotype characterized by skin laxity and fragility, reminiscent of certain human Ehlers-Danlos syndromes (EDSs), was observed in mice deficient in decorin, the most abundant SLRP in skin.<sup>(18)</sup> Likewise, mice deficient in lumican (an SLRP enriched in the cornea) develop corneal opacity.<sup>(19)</sup> In contrast, a skeletal phenotype characterized by growth failure, reduced bone formation, and osteopenia has been described recently in *bgn*-deficient mice.<sup>(20)</sup> Ultrastructural anomalies of dermal and corneal collagen fibrils have been observed in *dcn* and lumican-deficient mice but have not been reported in *bgn*-deficient animals.

The studies described here were designed to learn more about the role of *bgn* in connective tissue matrices, including nonskeletal tissues in which macroscopic abnormalities are not observed in the *bgn*-deficient mice. Toward this goal, we examined the ultrastructural morphology of collagenous matrices in *bgn*-deficient mice in comparison with *dcn*-deficient and wild-type (WT) animals. To further investigate the potential interplay of *bgn* and *dcn* in bone and other connective tissues, we generated *bgn* and *dcn* double-deficient mice. This allowed us to investigate the effects of biglycan deficiency in a decorin-deficient as well as in a decorin-sufficient background.

## MATERIALS AND METHODS

### Animals and tissues

All experiments using mice were performed under an institutionally approved protocol for the use of animals in research (NIDCR-IRP-98–058). The *dcn*- and *bgn*-deficient animals were generated as described.<sup>(18,20)</sup> Animals deficient in both *dcn* and *bgn* were generated as detailed in the following section. Male mice were used in this study. Throughout the text we have designated mice with genotype *dcn*<sup>−/−</sup> as *dcn* deficient or knockout (KO); *bgn*<sup>−/0</sup> as *bgn* deficient or KO; *dcn*<sup>−/−</sup>, *bgn*<sup>−/0</sup> as double-KO; and *bgn*<sup>+/0</sup>,

*dcn*<sup>+/+</sup> as WT. Data presented were from littermates from the F2 generation.

### Generation of *bgn*/*dcn*-deficient mice

Heterozygous *dcn*-deficient (−/+) male mice were crossed with homozygous *bgn*-deficient (−/−) female mice. F1 male mice with the genotype *dcn* (−/+) *bgn* (−/0) (designated as such because there is no allele on the Y chromosome) were bred to female mice with the genotype *dcn* (−/+) *bgn* (−/+) to generate F2 animals. Mice deficient in both *bgn* and *dcn* were identified by polymerase chain reaction (PCR) using DNA extracted from a 3-mm tail biopsy specimen with the Highpure PCR Template Preparation Kit (Boehringer Mannheim, Indianapolis, IN, USA). To identify the normal and targeted *dcn* alleles, three oligonucleotide primers were used: a forward primer corresponding to the 5' end of exon two (5'-cctctggcacaagtctcttg-3'; accession no. NM 007833, bases 255–276) and a reverse primer encoding either the 3' end of exon two (5'-tcgaagatgacactggcatcgg-3'; accession no. NM007833, reverse and complement of bases 324–405) or a primer with sequences within the phosphoglycerate kinase (PGK) promoter (5'-tgatgtggaatgtgtgcagg-3') of the targeted allele (Genbank accession no. AF090454, bases 1901–1922). Ten microliters of purified DNA (10–100 ng) were used as a template for the PCR reactions, which contained 2 ng/ $\mu$ l of each primer, 0.2 mM of deoxynucleoside triphosphate (dNTP) and a 1 $\times$  PCR buffer supplemented with 1.5 mM of MgCl (Applied Biosystems, Philips, Eindhoven, The Netherlands). After incubation of the reaction mixture at 95°C, a 0.5- $\mu$ l aliquot of Amplitaq gold (Applied Biosystems) was added to a total volume (TV) of 50  $\mu$ l and the reaction was allowed to proceed for 35 cycles at 95°C for 1 minute, 57°C for 20 s, and 72°C for 30 s. PCR products were resolved by electrophoresis through 1.8% agarose gels, yielding bands that were 161 bp for WT and 238 bp for targeted *dcn* alleles. Genotyping the *bgn* alleles used a similar strategy. In addition to the PGK primer described previously, a forward primer corresponding to the 5' end of exon two (5'-caggaa-cattgaccatg-3'; Genbank accession no. NM007542, bases 126–142) and a reverse primer corresponding to the 3' end of exon two (5'-gaaaggacacatggcactgaag-3'; Genbank accession no. NM007542, reverse and complement of bases 316–337) were used as described previously. Diagnostic bands of 212 bp and 310 bp represent the WT and targeted *bgn* allele, respectively. Out of 150 mice tested, only 5 were double KO; this is considerably lower (~3.3%) than expected for Mendelian inheritance (12.5%) using this breeding regime.

### X-ray studies and histology

Mice were killed at 2–5 months and hard tissues (femur and tibia) were dissected and soft tissues were removed. Femora were radiographed using a Faxitron MX-20 Specimen Radiography System (Faxitron X-ray Corp., Wheeling, IL, USA) at energy of 30 kV for 30 s. The images were captured with Eastman Kodak Co. X-OMAT TL (Eastman Kodak Co., Rochester, NY, USA). Both soft (ventral skin and tail tendon) and hard tissue samples were fixed with

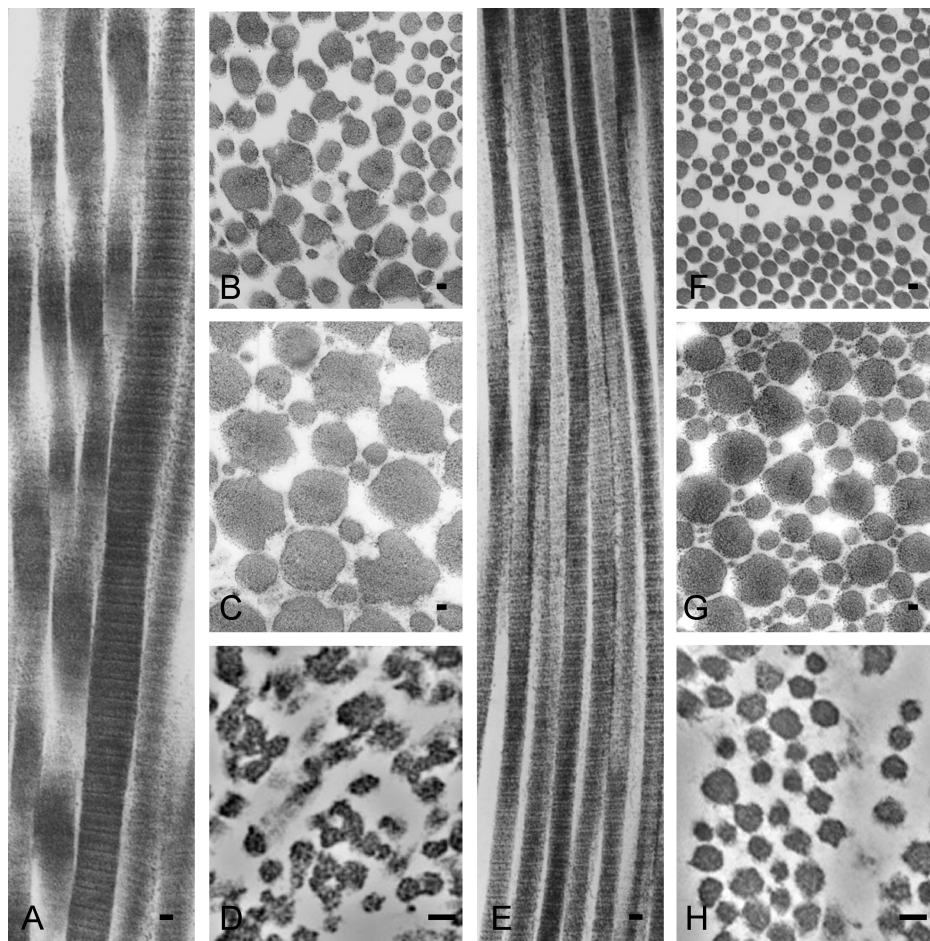


**FIG. 1.** (A, B, E, and F) Ultrastructural morphology of collagen fibrils from dermis, (C and G) tail tendon, and (D and H) bone from (A–D) *bgn*-deficient and (E–H) WT mice. (A) The variability along the individual fibril axis is illustrated by longitudinal sections of dermal collagen fibrils. Compared with (F–H) cross-sections of collagen fibrils of WT, in which profiles are circular and outlines are regular, (B–D) cross-sections of collagen fibrils of *bgn*-deficient mice reveal a greater variability in size and shape. Irregular cross-sectional profiles, indicative of abnormal lateral association or defective molecular rearrangement after fusion, are evident in all *bgn*-deficient tissues (bar = 50 nm).

fresh 4% formalin in 0.1 M of phosphate buffer, pH 7.2, for 16 h at 4°C. After washing, tissues were stored in 70% ethanol before embedding and processing. Samples from ventral skin and tail were embedded routinely in paraffin. Five-micrometer-thick paraffin sections were stained with hematoxylin-eosin or Mallory's trichrome. The right femora and tibiae were divided into proximal and distal halves and embedded undecalcified in glycol-methacrylate (GMA).<sup>(21)</sup> Three-micrometer-thick GMA sections were stained with May Grunwald-Giemsa or von Kossa.

Histomorphometry was performed with a semiautomatic image analyzer (IAS 2000; Delta System, Rome, Italy). Three animals of each strain were used to measure dermal thickness ( $\mu\text{m}$ ) and bone volume/TV (BV/TV, %). Dermal thickness was established by measuring five distances from the dermo-epidermal junction to the lower end of the dermis in ten adjacent fields by objective 10 $\times$  (on screen area 0.21 mm<sup>2</sup>). BV/TV was determined as described previously.<sup>(20)</sup> The data are expressed as mean  $\pm$  SD.

#### Transmission electron microscopy

Samples obtained from the ventral skin, tail tendon, and the left tibiae of 2-month-old mice of each strain were subjected to transmission electron microscopy (TEM) analysis. Before embedding, the tibia was divided into halves;

the proximal half was left undecalcified and the distal half was decalcified in neutral buffered 10% EDTA. After washing in PBS, the samples were postfixed for 1 h at 4°C with 1% osmium tetroxide in cacodylate buffer, rinsed in water, dehydrated through graded ethanol solutions, transferred to propylene oxide, and embedded in epoxy resin (Araldite). Semithin sections were stained with Azur II-Methylene Blue and examined with a light microscope to select appropriate fields; ultrathin sections were contrasted with uranyl acetate and lead citrate and examined with a CM 10 Philips electron microscope (KE Electronics, Tofts, UK).

Multiple micrographs of cross-sections of dermal, tail tendon, and nonmineralized-bone collagen fibrils were chosen randomly and used for morphometry. Mean diameter, range, and frequency distribution profiles were obtained by measuring manually the biggest diameter of 2000 collagen fibrils from each tissue.

#### Scanning electron microscopy

Dehydrated samples from the left femora were embedded in polymethyl methacrylate (PMMA) and the blocks were trimmed, micromilled to a  $\leq 0.1\text{-}\mu\text{m}$  relief, prepared, polished, and carbon-coated as described.<sup>(22)</sup> Quantitative backscattered electron (qBSE) imaging and the density of mineralization of the bone tissue were evaluated in a digital

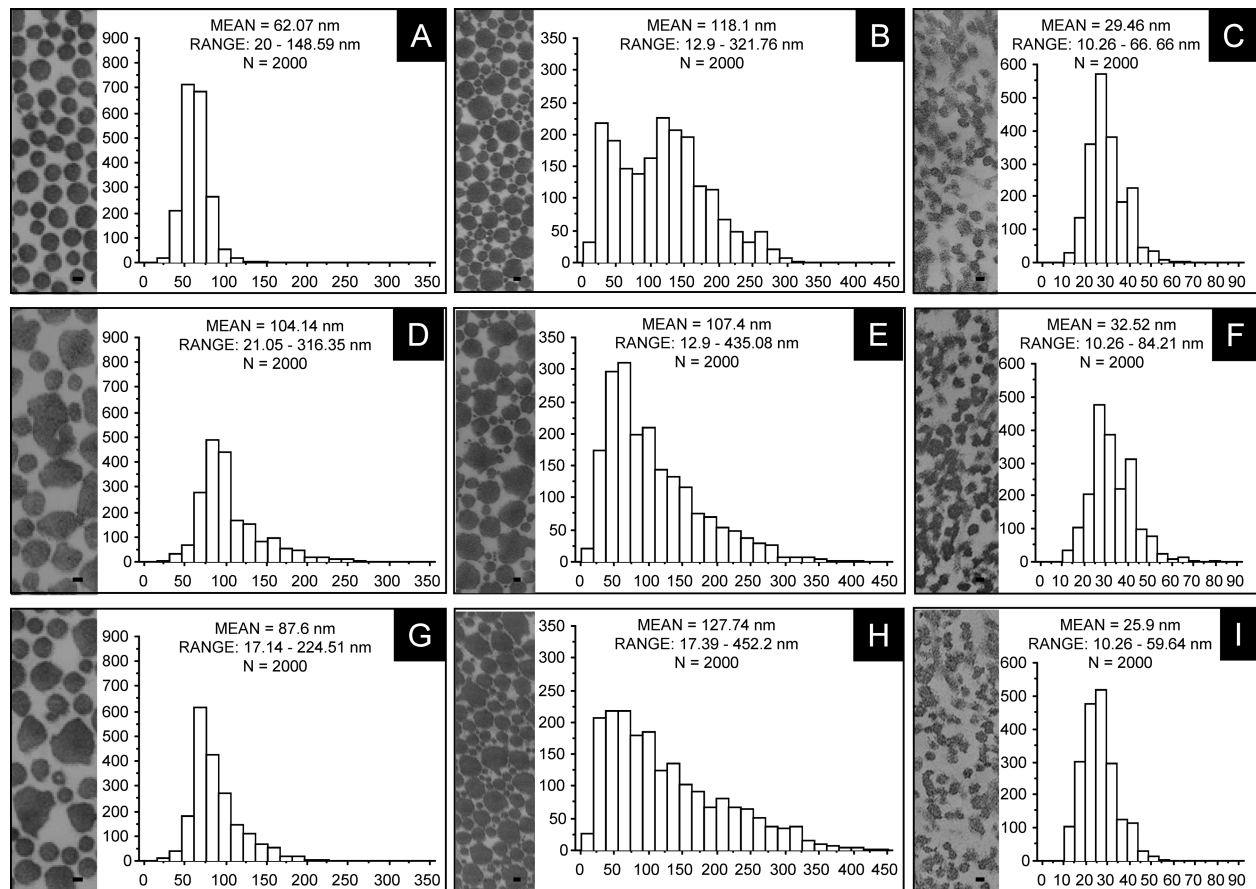


**FIG. 2.** TEM of cross-sections of collagen fibrils from (A, D, and G) skin, (B, E, and H) tail tendon, and (C, F, and I) bone and their frequency distribution from 2-month (A–C) WT, (D–F) *bgn*-deficient, and (G–I) *dcn*-deficient mice. In the dermis and in the tendon of both mutant mice, the great variability in fibril shape and diameter is evident and clearly proven by the increase in the range of collagen fibril size in both tissues and by the loss of the bimodal profile in the tendon. In bone, the mean fibril diameter and range are reduced in the *dcn* KO mice, whereas both are higher in the *bgn* KO mice compared with WT mice (bar = 50 nm in panels A, C, D, F, G, and I and 100 nm in panels B, E, and H).

scanning electron microscope (SEM) (Zeiss DSM 962 with Kontron IBAS external control computer) operating under standardized conditions.<sup>(23–25)</sup>

## RESULTS

### *Biglycan deficiency induces changes in collagen fibril morphology*

TEM studies of skin, tendon, and bone samples of *bgn*-deficient mice (Fig. 1) revealed the occurrence of a host of collagen fibril anomalies, including changes both in fibril size and in fibril shape. In all tissues, a marked variability of fibril diameter and the frequent occurrence of fibrils with an irregular cross-sectional profile (with a ragged or notched contour) were observed. Longitudinal sections of collagen fibrils also showed the occurrence of marked diameter variability along an individual fibril axis (so-called twisted fibrils) in mutant mice.

### *Collagen abnormalities induced by biglycan or decorin deficiency are different in different tissues*

On the whole, the collagen fibril abnormalities observed in *bgn*-deficient mice were qualitatively similar to those

previously described in the skin and tendon of decorin-deficient mice.<sup>(18)</sup> However, the overall phenotypes resulting from either decorin or biglycan deficiency are quite distinct (skin fragility vs. osteopenia<sup>(18,20)</sup>). Therefore, we comparatively analyzed fibril morphology, average diameter, range, and frequency distribution in skin, tail tendon, and bone from the two strains of mutant mice (Fig. 2).

Dermal collagen fibrils of WT animals had an average diameter of 62.07 nm with a range of 20–148.59 nm. Both *bgn* deficiency and *dcn* deficiency produced, in the dermis, an increase in fibril average diameter (*bgn*, 104.14 nm; *dcn*, 87.6 nm) and range (*bgn*, 21.05–316.35 nm; *dcn*, 17.14–224.51 nm) compared with WT animals. Fibrils with an unusually high diameter were apparent both in *bgn*- and *dcn*-deficient animals. The larger fibrils often exhibited an irregular cross-sectional profile. Consequently, at the TEM level, the effect of *bgn* deficiency (wider-size range and higher average diameter of collagen fibrils) was similar to the effect of *dcn* deficiency.

The tail tendon of WT animals contained two discrete main populations of fibrils, (30–60 nm and 100–150 nm in diameter, respectively) resulting in a typical bimodal profile of frequency distribution. Both in the *bgn*-deficient animals

and in the *dcn*-deficient animals, fibril diameter exhibited instead a unimodal frequency distribution because of a relative decrease in number of larger fibrils and a relative increase in number of smaller fibrils. The fibril size range was increased compared with WT animals (12.9–321.76 nm) both in the *bgn*-deficient animals (12.9–435.08 nm) and in the *dcn*-deficient animals (17.39–452.2 nm), reflecting the occurrence of unusually large fibrils. The average diameter of tendon collagen fibrils was reduced in the *bgn*-deficient mice (107.4 nm) and increased in the *dcn*-deficient mice (127.74 nm), compared with WT animals (118.1 nm).

In bone from WT animals, collagen fibrils had an average diameter of 29.46 nm with a range of 10.26–66.66 nm. Both *bgn* and *dcn* deficiency had an effect on fibril structure

and size. However, the effect was not the same in either case. In the *bgn*-deficient mice, both the fibril average diameter (32.52 nm) and the range (10.26–84.21 nm) were increased compared with WT mice. In the decorin-deficient mice, conversely, both the average diameter (25.9 nm) and the size range (10.26–59.64 nm) were decreased compared with WT mice. Irregular cross-sectional profiles were more obvious in the *bgn*-deficient mice.

#### *Bgn* deficiency and *dcn* deficiency induce subtle phenotypes in skin and bone, respectively

Because collagen fibril abnormalities observed in the skin of *bgn*-deficient mice were similar to those observed in *dcn*-deficient mice, we investigated the potential occurrence of a gross or histological cutaneous phenotype in *bgn*-deficient mice. In 2-month-old *dcn*-deficient mice, simple manual stretching was sufficient to produce a rupture of the skin (dermatosparaxis), as previously reported.<sup>(18)</sup> Similar maneuvers never produced any tearing of the skin in the *bgn*-deficient mice or in WT animals. However, histological evaluation of skin samples from both strains of mutant mice showed a similar reduction in the thickness of the dermis compared with WT animals (Fig. 3). We concluded from these observations that collagen anomalies are reflected in an overt dermatosparaxis-like phenotype in the *dcn*-deficient, *bgn*-sufficient mice, but only in a subtle, “subclinical” cutaneous phenotype in *bgn*-deficient, *dcn*-sufficient mice.

Because *dcn* deficiency induced a detectable change in collagen fibril size and shape in bone, we asked whether a subtle skeletal phenotype could be shown in *dcn*-deficient mice. No reduction in skeletal mass similar to the previously reported skeletal phenotype of *bgn*-deficient mice was observed in the *dcn*-deficient mice on by X-ray analysis, histological examination, or histomorphometric assessment of trabecular bone mass (BV/TV%, Fig. 4). Thus, we concluded that decorin deficiency only induced an EM-detectable phenotype in bone, with no expression at the histological or gross level.

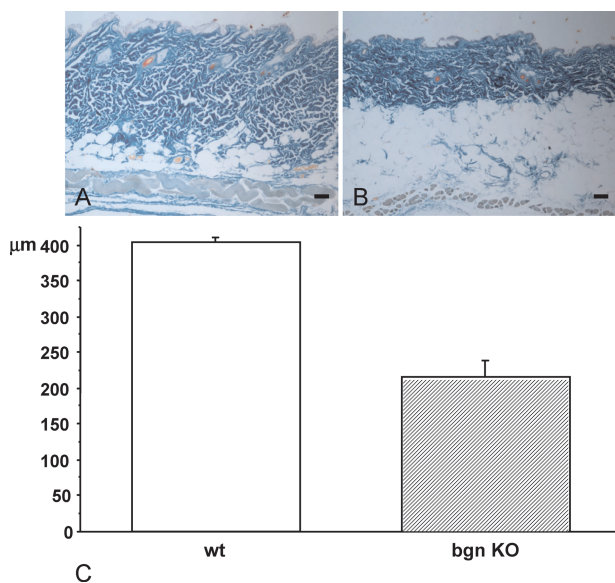


**FIG. 3.** Skin histology of (A) WT and (B) *bgn* KO mice and (C) comparison (mean  $\pm$  SD) of dermal thickness. Thinning of the dermis is evident in *bgn* KO mice (bar = 50  $\mu$ m).

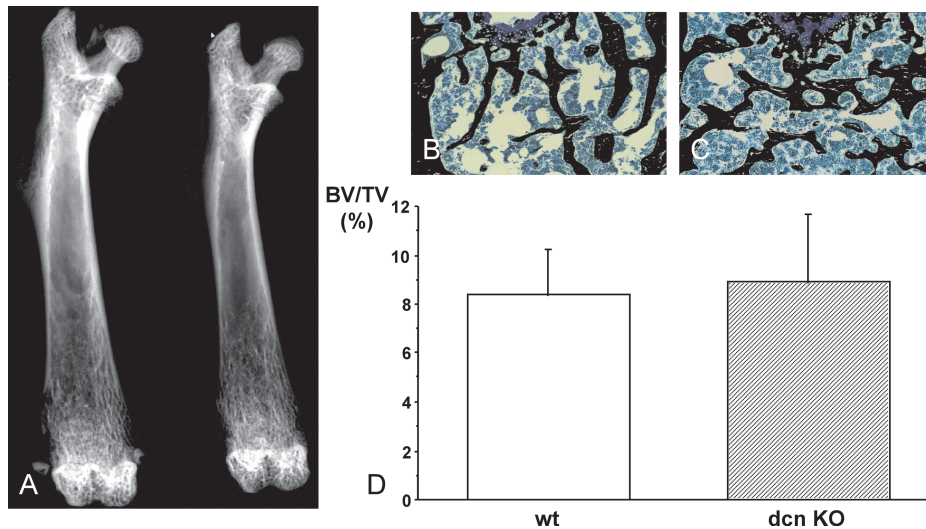


**FIG. 4.** Comparative X-rays of the (A) whole femur and histology of distal femur after von Kossa staining of (B) WT mice and (C) *dcn* KO mice and their (D) BV/TV quantitation. No reduction in bone mass is evident in *dcn* KO mice at any level of analysis.

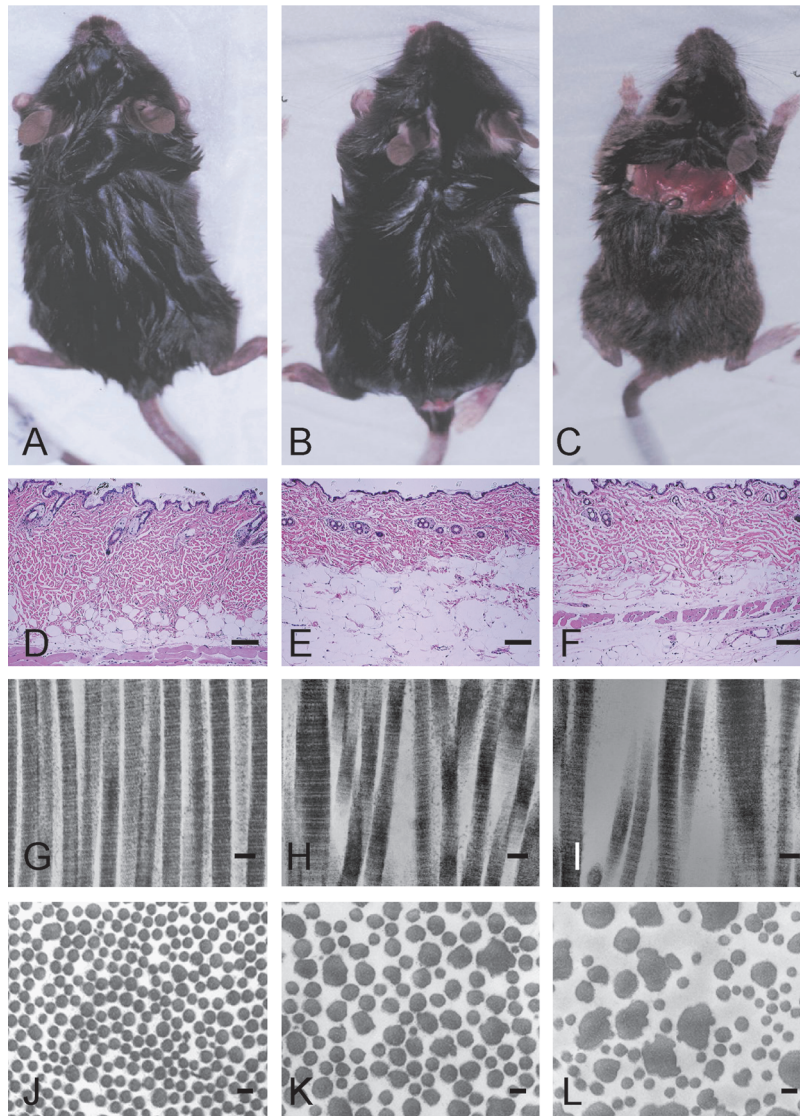


**FIG. 5.** (A–C) Mice, (D–F) skin histology, and (G–I) longitudinal and (J–L) cross-sectional TEM morphology of collagen fibrils of (A, D, G, and J) WT mice, (B, E, H, and K) *dcn* KO mice, and (C, F, I, L) *bgn/dcn* double-deficient mice. (B) Rupture of the coat wider than that observed in *dcn* KO mice is evident in (C) *bgn/dcn* double-KO mice. (E) Thinning of the dermis is evident in *dcn* KO mice and looseness and (F) disorganization of dermal collagen bundles and the absence of a well-formed hypodermal layer are observed only in the double-KO mice. Comparative TEM analysis of dermal collagen shows more marked variability in fibril size and shape and wider interfibrillar spaces in (I and L) *bgn/dcn* KO mice compared with (G and J) WT mice and (H and K) *dcn* KO mice (bar = 100  $\mu$ m in panels D–F and 100 nm in panels G–L).

#### *Decorin deficiency enhances skeletal and extraskelatal effects of biglycan deficiency*

To investigate the potential skeletal and extraskelatal effects of biglycan deficiency in a decorin-deficient background (and vice versa), we generated *bgn/dcn* double-KO animals. A dermatosparaxis-like gross phenotype was prominent in the double mutant, with tearing of the coat occurring even after gentle stretching (Fig. 5). Ruptures were consistently wider than in the *dcn*-deficient mice.

Histologically, the skin of double-deficient animals showed a thinned dermis, compared with WT animals, like *bgn*- and *dcn*-deficient mice, and showed, in addition, two specific qualitative differences. The texture of dermal collagen was obviously looser, with wide spaces separating collagen bundles. In addition, the hypodermis was uniformly atrophic. Ultrastructural analysis of the dermal collagen showed that double-SLRP deficiency resulted in a more marked variability in fibril size (reflected in a wider range of fibril diameter: 22.86–422.91 nm, average 91.99 nm) compared with WT, *bgn*-deficient, and

*dcn*-deficient animals. In addition, fibrils were markedly less tightly packed with wide interfibrillar spaces, and fibril cross-sectional profiles often were ragged or notched but still predominantly circular.

Double-deficient animals exhibited a striking and early appearing gross skeletal phenotype (Fig. 6). Long bones were shorter and wider compared with WT animals and markedly osteopenic on X-ray and histological and SEM analysis. At 2 months of age, when osteopenia is barely discernible in *bgn*-deficient animals,<sup>(20)</sup> cortical and trabecular bone mass clearly was reduced severely in double-deficient animals compared with WT animals (BV/TV%, mean  $\pm$  SD: double-KO mice,  $1.61 \pm 0.12$  and  $n = 3$ ; WT,  $8.39 \pm 1.85$  and  $n = 3$ ). In bone, *bgn* and *dcn* double deficiency resulted in a striking change in collagen fibril shape and organization (Fig. 7). In single mutant animals, fibrils still were predominantly circular in cross-section (despite an irregular, ragged, or notched profile) and of an altered size. No circular cross-sectional profiles could be observed at all in double-deficient animals, and fibrils uni-

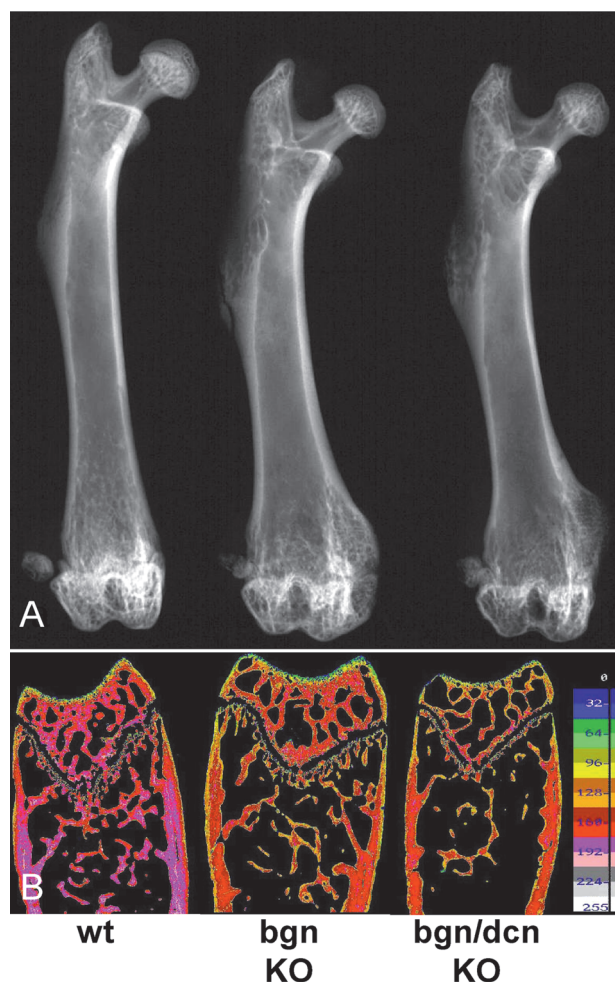


**FIG. 6.** (A) Comparative X-rays of the whole femur and (B) qBSE analysis of the left distal femur from 2-month WT mice, *bgn* KO mice, and *bgn/dcn* KO mice. Cortical and trabecular bone mass clearly was reduced severely at 2 months of age in double-deficient animals. A reduced mineral content (as indicated by the pseudocolor scale, in which higher values are at the bottom) is observed both in the *bgn* and in the *bgn/dcn* double-deficient animals compared with WT animals.

formly displayed a marked “serrated” appearance, with a variety of shapes merging in places with a true “hieroglyphic-like” morphology (as described in certain human EDSs and animal correlates thereof<sup>(26–32)</sup>). Interfibrillar space appeared to be widened in thin sections from samples routinely processed for EM, suggesting a reduction in overall collagen mass. Interestingly, the typical collagenous texture observed in normal bone by BSE imaging was completely lost in bones from double-deficient animals and replaced by a uniform, glassy appearance of the mineralized matrix in polished and coated samples (Fig. 7).

## DISCUSSION

### *BGN is an important determinant of collagen fibril assembly in vivo*

Fibrillar collagens constitute the bulk of all connective tissues and provide the basis for the tensile properties as

well as the biomechanical support for optimal function of these tissues. Based on a number of in vitro observations, the assembly and structure of collagen fibrils have long been thought to be modulated via interaction of fibrillar collagens with a number of macromolecules, including different types of collagens, noncollagenous glycoproteins, and proteoglycans.<sup>(9–16,33,34)</sup> SLRPs are important members of the host of potential collagen binders/regulators, and in vitro data supporting such a role are available for most, if not all, SLRPs. Direct in vivo evidence for a role of some SLRPs in regulation of collagen assembly has been offered by the recent development of mice deficient in *dcn*, lumican, and fibromodulin, three distinct members of the SLRPs family. In all of these animals, collagen fibril anomalies have been noted in different tissues.<sup>(18,19,35,36)</sup> An analysis of collagen fibrils in the osteopenic *bgn*-deficient mice, conversely, had not been conducted previously. The data reported in this study establish that *bgn* plays a critical role in the regulation of collagen architecture and structure in vivo. *Bgn* deficiency results in formation of collagen fibrils noted for an irregular profile, a broader-size range, and less tight packing. These changes are not restricted to the skeleton and are generalized to diverse type I collagen-rich connective tissues.

### *Similar and additive effects of bgn and dcn deficiency in the dermis*

In different tissues, the effects of biglycan deficiency may either translate into a macroscopic phenotype (as in bone) or be apparent at the ultrastructural and histological level only, as in skin. *Bgn* deficiency produces collagen abnormalities and thinning of the dermis but does not convey overt skin fragility. Although the observed ultrastructural and histological changes do predict a subtle degree of skin fragility, *bgn*-deficient mice are not dermatosparactic. Their skin might prove less resilient on biomechanical testing and yet does not rupture on simple manipulation, as is the case in animals with spontaneous or experimental dermatosparaxis, including *dcn*-deficient mice. Thus, *Bgn* and *dcn* deficiency seem to produce similar ultrastructural and histological changes in the skin but only *dcn* deficiency is apparently effective in inducing a dermatosparaxis-like phenotype. A macroscopically apparent effect implies a more severe impact on matrix organization than changes detected by EM or histology only. The greater impact of *dcn* deficiency versus *bgn* deficiency on skin integrity thus remains consistent with the greater relative abundance of *dcn* in the dermis, whereas the similarity in ultrastructural changes produced by either type of SLRP deficiency is consistent with an overall similar role of *bgn* and *dcn* in interactions with dermal collagen. In agreement with this interpretation, the effects of double-*bgn* and -*dcn* deficiency, as observed in the double-KO mice, are additive. In these animals, ultrastructural changes in dermal collagen are more pronounced than in either single mutant animals and extensive ruptures of the skin are produced even by gentle manipulation.

### *Distinct and synergic effects of bgn and dcn deficiency in bone*

Although both *bgn* and *dcn* deficiency affect collagen fibril size and shape in bone, they do so in a markedly

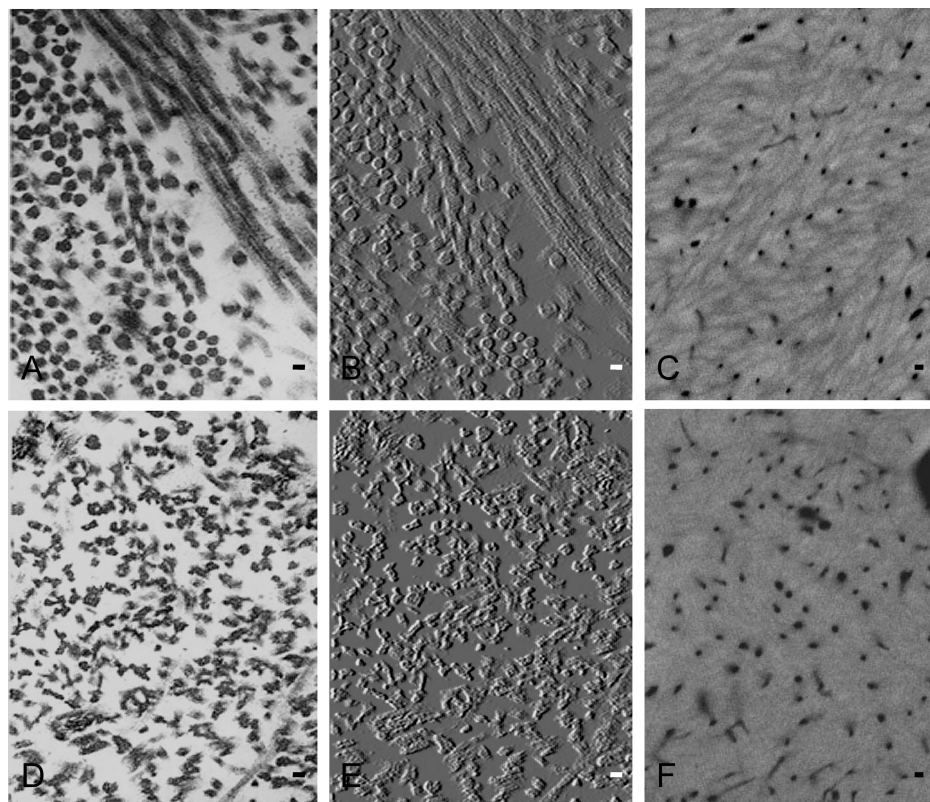


**FIG. 7.** EM images of cross-sections of collagen fibrils of bone tissue from 2-month (A–C) WT and (D–F) *bgn/dcn* KO mice. (B and E) The same images as shown in panels A and D, modified using Adobe Photoshop 5.0 to better visualize fibril profile features. (D and E) No circular cross-sectional profiles are evident in double-deficient animals and fibrils uniformly show a marked serrated appearance highly reminiscent of hieroglyphics. (C) The typical collagenous texture observed in WT bone by BSE imaging is completely lost in (F) double-deficient animals in which the mineralized matrix appears uniformly glassy (bar = 50 nm in panels A, B, D, and E and 50  $\mu$ m in panels C and F).

different and, in fact, opposite way. Fibril average diameter and size range increase as an effect of *bgn* deficiency and decrease as an effect of *dcn* deficiency, compared with WT animals. Because *dcn* deficiency results in larger fibrils in the dermis (and tendon), the effects of *dcn* deficiency on collagen fibril structure in bone seem to be rendered distinct and specific by the local matrix environment. Although the cutaneous phenotypes of *bgn*- and *dcn*-deficient mice are grossly distinct but histologically and ultrastructurally similar to one another, the skeletal phenotypes of *bgn*- and *dcn*-deficient mice differ from one another at all levels of investigation. *Dcn*-deficient mice do not feature the osteopenia of *bgn*-deficient mice either at the gross or at the histological level and exhibit distinct ultrastructural changes in bone collagen fibrils. Double-deficient mice display a unique ultrastructural phenotype in bone, noted for the almost complete loss of fibril basic geometry. Very few fibrils in the double-KO mice exhibit a predominantly circular cross-sectional profile, and the vast majority of the fibrils provide a noted example of the so-called “serrated” fibril morphology observed in many human disorders, first and foremost the varied spectrum of EDSs.<sup>(26–30)</sup> In the bone matrix of double-KO mice, the cross-sectional profile of collagen fibrils approaches the hieroglyphic-like pattern described for skin collagen in human dermatosparaxis and makes it hard to determine and measure their diameter. This ultrastructural phenotype is matched by a markedly osteopenic gross phenotype, which compared with the phenotype of *bgn* single-deficient mice is more severe and appears at an earlier animal age. Thus, *dcn* deficiency synergizes with *bgn* deficiency in producing a skeletal phenotype al-

though the effects of individual *dcn* and *bgn* deficiencies in bone are quite distinct.

Finally, further studies are desirable to clarify the mechanisms by which the effects of *bgn* and *dcn* deficiency are similar and additive in the dermis and distinct and synergic in bone. Either the unique complement of other noncollagenous proteins found in both tissues or tissue-specific features of type I collagen or differences in the ratios of type I, type III, and type V collagen might reflect in diverse tissue-specific collagen-SLRP interaction and in tissue-specific effects of their disruption.

#### Relationship to human EDSs

Previously, the similarity between the cutaneous phenotype of the *dcn*-deficient mice with the cutaneous expression of human EDSs and relevant animal correlates has been noted.<sup>(18)</sup> Human EDSs comprise a markedly heterogeneous group of disorders, in which clinical heterogeneity reflects the varied expressivity in different tissues of multiple genetic defects, most of which involve collagen type I genes.<sup>(37)</sup> Changes in collagen fibrils occurring in human EDSs (variability in size and density, ragged profiles, “serrated” fibrils, and twisted fibrils) are closely similar to those observed in mice deficient in *bgn*, *dcn*, and other SLRPs. In addition to skin laxity or fragility, joint laxity and vascular fragility also characterize, clinically, certain EDSs. Curiously, all these cardinal elements of the EDSs as a group also have been reproduced by a spectrum of mouse models of SLRP deficiencies, including skin fragility,<sup>(18,19)</sup> joint laxity,<sup>(38)</sup> and vascular fragility (our unpublished data). The

original analogy between murine decorin deficiency<sup>(18)</sup> and human cutaneous ED now can be broadened and reasonably elaborated as a working hypothesis in a more general paradigm, in which multiple forms of human EDSs and multiple murine models of SLRP deficiency may be inscribed. However, most ED variants are not recognized generally as typically associated with an overt skeletal pathology. This would leave the osteopenic biglycan-deficient animals (both the *bgn* KO model and the *bgn/dcn* double-KO model) outside of the envisioned paradigm. However, there have been repeated indications for variable degrees of osteopenia in patients with EDSs.<sup>(39)</sup> Furthermore, osteopenia is a recognized integral part of one specific subtype of human EDS (the progeroid variant, OMIM 130070). This rare disorder is the phenotypic consequence of a defective gene encoding xylosylprotein 4- $\beta$ -galactosyltransferase I,<sup>(40,41)</sup> resulting in the production of *BGN* and *DCN* core proteins with a deficiency of GAG chain attachment. In this EDS variant, osteopenia is in fact observed in conjunction with growth failure, skin fragility, and cutaneous changes resembling those observed in progeria. Of note, skin fragility and growth failure are observed in the *dcn/bgn* double-KO mice. These mice also show a distinctive atrophy of the subcutis, which in humans represents the hallmark of true progeria that is mimicked in the progeroid variant of EDS. Thus, it seems reasonable to propose that depletion of both *dcn* and *bgn* in the double-KO mice results in a murine model of a human condition in which GAG-deficient DCN and BGN are produced, and a combined deficiency of both glycosylated BGN and glycosylated DCN occurs. If so, one would infer that either the stabilization or the interaction properties of DCN and BGN would indeed be dependent on efficient GAG attachment.

It is important to note, from a general point of view that all other known mutations underlying human EDSs occur in genes encoding either collagen chains (types I, III, and V) or collagen-processing enzymes (*N*-propeptidase and lysyl-hydroxylase).<sup>(37)</sup> Marked alterations in the organization of collagenous matrices result from these mutations and mediate the disease phenotypes. However, collagen is not the only determinant of the overall organization of collagenous matrices. As emphasized by our data and those of others, SRLP deficiencies obviously generate changes in the organization and structure of collagen fibrils, which translate into abnormal phenotypes reminiscent of various EDS-like conditions. Because not all human EDSs necessarily reflect mutations in collagen genes and the gene defect underlying certain variants remain unknown, SLRP-encoding genes emerge as potential candidate genes for subsets of human EDSs or related conditions, which remain to be identified.<sup>(30)</sup>

## ACKNOWLEDGMENTS

This work was supported in part by grants from the Ministry for University and Research (MIUR), Italy (to P.B.).

## REFERENCES

1. Fisher LW, Termine JD, Dejter SW Jr, Whitson SW, Yanagishita M, Kimura JH, Hascall VC, Kleinman HK, Hassell JR, Nilsson B 1983 Proteoglycans of developing bone. *J Biol Chem* **258**:6588–6594.
2. Fisher LW, Termine JD, Young MF 1989 Deduced protein sequence of bone small proteoglycan I (biglycan) shows homology with proteoglycan II (decorin) and several nonconnective tissue proteins in a variety of species. *J Biol Chem* **264**:4571–4576.
3. Hocking AM, Shinomura T, McQuillan DJ 1998 Leucine-rich repeat glycoproteins of the extracellular matrix. *Matrix Biol* **17**:1–19.
4. Iozzo RV 1998 Matrix proteoglycans. From molecular design to cellular function. *Ann Rev Biochem* **67**:609–652.
5. Geerkens C, Vetter U, Just W, Fedarko NS, Fisher LW, Young MF, Termine JD, Robey PG, Wohlr D, Vogel W 1995 The X-chromosomal human biglycan gene *BGN* is subject to X inactivation but is transcribed like an X-Y homologous gene. *Hum Genet* **96**:44–52.
6. Hausser H, Groning A, Hasilik A, Schonherr E, Kresse H 1994 Selective inactivity of TGF- $\beta$ /decorin complexes. *FEBS Lett* **353**:243–245.
7. Ruoslahti E 1989 Proteoglycans in cell regulation. *J Biol Chem* **264**:13369–13372.
8. Iozzo RV 1999 The biology of the small leucine-rich proteoglycans. Functional network of interactive proteins. *J Biol Chem* **274**:18843–18846.
9. Vogel KG, Trotter JA 1987 The effect of proteoglycans on the morphology of collagen fibrils formed in vitro. *Coll Relat Res* **7**:105–114.
10. Hedbom E, Heinegård D 1993 Binding of fibromodulin and decorin to separate sites on fibrillar collagens. *J Biol Chem* **268**:27307–27312.
11. Rada JA, Cornuet PK, Hassell JR 1993 Regulation of corneal collagen fibrillogenesis in vitro by corneal proteoglycan (lumican and decorin) core proteins. *Exp Eye Res* **56**:635–648.
12. Kresse H, Hausser H, Schonherr E, Bittner K 1994 Biosynthesis and interactions of small chondroitin/dermatan sulphate proteoglycans. *Eur J Clin Chem Clin Biochem* **32**:259–264.
13. Schonherr E, Hausser H, Beavan L, Kresse H 1995 Decorin-type I collagen interaction. Presence of separate core protein-binding domains. *J Biol Chem* **270**:8877–8883.
14. Schonherr E, Witsch-Prehm P, Harrach B, Robenek H, Rautenberg J, Kresse H 1995 Interaction of biglycan with type I collagen. *J Biol Chem* **270**:2776–2783.
15. Kadler KE, Holmes DF, Trotter JA, Chapman JA 1996 Collagen fibril formation. *Biochem J* **316**:1–11.
16. Kuc IM, Scott PG 1997 Increased diameters of collagen fibrils precipitated in vitro in the presence of decorin from various connective tissues. *Connect Tissue Res* **36**:287–296.
17. Bianco P, Fisher LW, Young MF, Termine JD, Robey PG 1990 Expression and localization of the two small proteoglycans biglycan and decorin in developing human skeletal and non-skeletal tissues. *J Histochem Cytochem* **38**:1549–1563.
18. Danielson KG, Baribault H, Holmes DF, Graham H, Kadler KE, Iozzo RV 1997 Targeted disruption of decorin leads to abnormal collagen fibril morphology and skin fragility. *J Cell Biol* **136**:729–743.
19. Chakravarti S, Magnuson T, Lass JH, Jepsen KJ, LaMantia C, Carroll H 1998 Lumican regulates collagen fibril assembly: Skin fragility and corneal opacity in the absence of lumican. *J Cell Biol* **141**:1277–1286.
20. Xu S, Bianco P, Fisher LW, Longenecker G, Smith E, Goldstein S, Bonadio J, Boskey A, Heegard AM, Sommer B, Satomura K, Dominguez P, Zhao C, Kulkarni AB, Gehron Robey P, Young MF 1998 Targeted disruption of the biglycan gene leads to an osteoporosis-like phenotype in mice. *Nat Genet* **20**:78–82.

21. Bianco P, Ponzi A, Bonucci E 1984 Basic and "special" stains for plastic sections in bone marrow histopathology, with special reference to May-Grunwald Giemsa and enzyme histochemistry. *Basic Appl Histochem* **28**:265–279.
22. Boyde A, Corsi A, Quarto R, Cancedda R, Bianco P 1999 Osteoconduction in large macroporous hydroxyapatite ceramic implants: Evidence for a complementary integration and disintegration mechanism. *Bone* **24**:579–589.
23. Boyde A, Davy KWM, Jones SJ 1995 Standards for mineral quantitation of human bone by analysis of backscattered electron images. *Scanning* **17**(Suppl V):6–7.
24. Howell PGT, Davy KWM, Boyde A 1998 Mean atomic number and backscattered electron coefficient for some materials with low atomic mean number. *Scanning* **20**:35–40.
25. Howell PGT, Boyde A 1998 Monte Carlo simulation of electron backscattering from compounds with low mean atomic number. *Scanning* **20**:45–49.
26. Holbrook KA, Byers PH 1982 Structural abnormalities in the dermal collagen and elastic matrix from the skin of patients with inherited connective tissue disorders. *J Invest Dermatol* **79**:7S–16S.
27. Kobayasi T, Oguchi M, Asboe-Hansen G 1984 Dermal changes in Ehlers-Danlos syndrome. *Clin Genet* **25**:477–484.
28. Steinmann B, Royce PM, Superti-Furga A 1993 The Ehlers-Danlos Syndrome. In: Royce PM, Steinmann B (eds.) *Connective Tissue and Its Heritable Disorders. Molecular, Genetic and Medical Aspects*. Wiley-Liss, Inc., New York, NY, USA, pp. 351–408.
29. Hausser I, Anton-Lamprecht I 1994 Differential ultrastructural aberrations of collagen fibrils in Ehlers-Danlos syndrome types I–IV as a means of diagnostics and classification. *Hum Genet* **93**:394–407.
30. Mao JR, Bristow J 2001 The Ehlers-Danlos syndrome: On beyond collagens. *J Clin Invest* **107**:1063–1069.
31. Hardy MH, Fisher KR, Vrablic OE, Yager JA, Nimmo-Wilkie JS, Parker W, Keeley FW 1988 An inherited connective tissue disease in the horse. *Lab Invest* **59**:253–262.
32. Brown PJ, Young RD, Cripps PJ 1993 Abnormalities of collagen fibrils in a rabbit with a connective tissue defect similar to Ehlers-Danlos syndrome. *Res Vet Sci* **55**:346–350.
33. Birk DE, Fitch JM, Babiarz JP, Doane KJ, Linsenmayer TF 1990 Collagen fibrillogenesis in vitro: Interaction of types I and V collagen regulates fibril diameter. *J Cell Sci* **95**:649–657.
34. Fleischmajer R, Perlsh JS, Burgeson RE, Shaikh-Bahai F, Timpl R 1990 Type I and type III collagen interactions during fibrillogenesis. *Ann NY Acad Sci* **580**:161–175.
35. Svensson L, Aszódi A, Reinholt FP, Fässler R, Heinegård D, Oldberg Å 1999 Fibromodulin-null mice have abnormal collagen fibrils, tissue organization, and altered lumican deposition in tendon. *J Biol Chem* **274**:9636–9647.
36. Ezura Y, Chakravarti S, Oldberg A, Chervoneva I, Birk DE 2000 Differential expression of lumican and fibromodulin regulate collagen fibrillogenesis in developing mouse tendons. *J Cell Biol* **151**:779–788.
37. Beighton P, De Paepe A, Steinmann B, Tsipouras P, Wenstrup RJ 1998 Ehlers-Danlos syndromes revised nosology, Villefranche, 1997. Ehlers-Danlos National Foundation (USA) and Ehlers-Danlos Support Group (UK). *Am J Med Genet* **77**:31–37.
38. Ameye L, Aria D, Chen X-D, Gehron Robey P, Chakravarti S, Oldberg A, Young MF 2000 Biglycan and fibromodulin double knockout mice develop ectopic sesamoid bones and premature osteoarthritis in the knee joint. *J Bone Miner Res* **15**:S1:185.
39. Dolan AL, Arden NK, Grahame R, Spector TD 1998 Assessment of bone in Ehlers Danlos syndrome by ultrasound and densitometry. *Ann Rheum Dis* **57**:630–633.
40. Kresse H, Rosthoj S, Quentin E, Hollmann J, Glossl J, Okada S, Tonnesen T 1987 Glycosaminoglycan-free small proteoglycan core protein is secreted by fibroblasts from a patient with a syndrome resembling progeroid. *Am J Hum Genet* **41**:436–453.
41. Quentin E, Gladen A, Roden L, Kresse H 1990 A genetic defect in the biosynthesis of dermatan sulfate proteoglycan. Galactosyltransferase I deficiency in fibroblasts from a patient with a progeroid syndrome. *Proc Natl Acad Sci USA* **87**:1342–1346.

Address reprint requests to:

*Marian Young, Ph.D.*

*Chief, Molecular Biology of Bones and Teeth Unit*

*Craniofacial and Skeletal Diseases Branch*

*Building 30, Room 225*

*National Institute of Craniofacial and Skeletal Diseases*

*Branch*

*MSC 4320*

*National Institutes of Health*

*Bethesda, MD 20892, USA*

Received in original form October 23, 2001; in revised form January 25, 2002; accepted February 6, 2002.